Quantitative structural characterization of InAs/GaSb superlattices

Ge "Joseph" Liu,[a] Bernd Fruhberger, and Ivan K. Schuller
Department of Physics, University of California-San Diego, La Jolla, California 92093

Heather J. Haugan and Gail J. Brown
Air Force Research Laboratory, Wright-Patterson AFB, Ohio 45433-7707

Molecular beam epitaxy grown InAs/GaSb superlattices, containing InSb-like interfacial layers, were analyzed by a combination of x-ray diffraction (XRD) and structural refinement. The superlattice refinement from x rays (SUPREX) method determines with high accuracy the average thicknesses and d spacings of the individual InAs and GaSb layers in addition to standard structural parameters usually obtained by XRD, such as the modulation length (periodicity), average out-of-plane interplanar spacings, and total thickness. The combined SUPREX/XRD experiments show that the absence of certain odd order satellite features in the x-ray data is due to asymmetric and inhomogeneous lattice strain. © *2006 American Institute of Physics*. [DOI: 10.1063/1.2353732]

I. INTRODUCTION

The material research and device design of high performance infrared detectors or lasers based on III–V semiconductor superlattices (SLs) have received significant attention in recent years. InAs/GaSb binary-binary type-II superlattices, which were proposed nearly 20 years ago,[1,2] are becoming a competitive alternative to silicon based or II–VI alloy based devices. Highly promising aspects of InAs/GaSb based devices include tunable band gaps, direct band transition, and reduced Auger recombination noise. Comprehensive photoresponse studies of the InAs/GaSb SL band gap were carried out by several groups[3–5] and the relevant theoretical analysis was also presented in several papers.[6,7] Previous studies show that the InAs/GaSb structure has a dominant effect on the band gap and photoresponse efficiency.[7,8] Thus it is important to understand the way in which the superlattice structure influences its physical properties. Local surface and cross-section morphology have been studied by transmission electron microscopy (TEM), atomic force microscopy (AFM) and scanning tunneling microscopy (STM). Structure parameters, such as the capping surface, buffer layer, and substrate roughness, and interlayer defect replication can be well studied with these methods.[8–10] Raman spectroscopy offers an alternative for the determination of chemical composition and bonding configuration, making it a major tool to understand the interfacial behavior of superlattices.[11] X-ray diffractometry (XRD) is a direct structural method useful for the determination of the global superlattice structure. Analysis of Ω-Θ/2Θ [Ω-dependent Θ-2Θ curves or two-dimensional (2D) scan] scans gives information along the layer-stacking z direction as well as the parallel xy direction. The modulation length (periodicity), the average out-of-plane interplanar spacings of bilayers, and the total thickness of InAs/GaSb superlattices can be readily obtained from typical XRD. However, further structure analysis requires the application of a structural "refinement" procedure such as SUPREX,[12–15] based on nonlinear optimization of structural models. In this paper, we apply SUPREX to InAs/GaSb superlattice samples and examine the validity of models with different strain profiles. We discuss the relevance of interfacial layers on the strain and the coherence using our refinement results.

II. EXPERIMENT AND FITTING PROCEDURE

The InAs/GaSb superlattices were fabricated by molecular beam epitaxy from elemental Ga and In, and valved cracker cells for As and Sb. The GaSb buffer layers were grown on Te-doped (1 0 0) GaSb substrates at a temperature of 500 °C. The growth temperature was then lowered to 400±5 °C for the SL layer growth. After SL growth, a 15 min *in situ* annealing at 450 °C under Sb overpressure was applied for the improvement of layer quality. The InSb-like interfacial layers were inserted between the main constituent layers of the SLs to modulate the SL strain to reach stress balance. The InSb-like interfacial layers were prepared by controlling the molecular beam epitaxy (MBE) shutter sequence.[16] All superlattices were grown with the same number of 20 periods.

X-ray diffraction data were acquired using two 1/6° slits to collimate the incident x-ray beam and two 0.3 mm wide slits on the outgoing beam to achieve higher momentum resolution. The Cu x rays were not monochromized, so that for sufficiently narrow intrinsic diffraction peaks the Cu $K\alpha_1$/Cu $K\alpha_2$ doublet was resolved. The setup allows selection of several acquisition modes, including Θ-2Θ, Ω, and Ω-Θ/2Θ (Ω-dependent Θ-2Θ curves or 2D scan) modes. The various angles of the x-ray diffraction experimental setup are defined in Fig. 1. The superlattices were aligned with the z direction, parallel to the x-ray momentum transfer.

The full Θ-2Θ scans of our samples can be divided into (0 0 0), (0 0 2), (0 0 4), and (0 0 6) ranges. Figure 2 shows Θ-2Θ scans of the (0 0 4) range of the six samples studied in this paper. From the bottom to the top they are labeled from 1 to 6, respectively, and are described in Table I. The data sets around the main diffraction peaks for the different
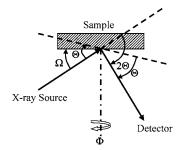
[a]Electronic mail: geliu@physics-mail.ucsd.edu

100, 063536-1

FIG. 1. Definition of angles in the x-ray diffraction experiment.

FIG. 2. Θ-2Θ coupled XRD results of (0 0 4) curves for a series of samples. From bottom to top, these curves are from the samples listed in Table I. Note the absence of some of the odd order peaks on the right hand side of the central peak.

ranges are simulated and analyzed using the SUPREX refinement package.[13–15] Because the particular method of preparation of the interfacial layers is expected to result in a continuous chemical transitional layer, we approximate it as an interdiffusion profile in our model. Thus the approach to structural refinement employs a bilayered superlattice model which includes a strain profile along the z direction. The details of the models and our refinement approach are detailed in Appendix A.

III. EXPERIMENTAL AND FITTING RESULTS

A. General observation and model selection

The thickness variations of the transitional InSb-like layer (treated as interdiffusion in our refinement) cause systematic changes in the XRD spectra of the superlattices (Fig. 2). In the sample with an intended abrupt interface (i.e., without an interfacial layer; second curve from the bottom), the zeroth order superlattice peaks are well separated from the GaSb buffer. This indicates that the average d spacing of the superlattice differs significantly from that of the GaSb bulk (arrow B in Fig. 2). As the thickness of the InSb-like interfacial layer is increased, the zeroth order (central) superlattice peaks move closer to the GaSb peaks (arrow C in Fig. 2), as has been observed before.[8,11]

In general, differences in bulk chemical, structural, and mechanical properties of constituent layers forming a superlattice may cause strain. This directly influences the position of the zeroth order peaks and the average d spacings of the InAs and GaSb constituents. Models with different out-of-plane strain profiles that can be conceived include (a) uniformly strained InAs and GaSb constituent layers and (b) unevenly strained constituent layers—the center parts of the layers are less strained with d spacings approaching that of
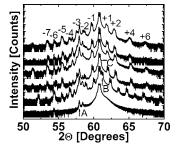
the bulk materials, and the boundary parts are more strained in order to balance stress across the layer boundary. Furthermore, the two boundaries at the bottom and at the top of each constituent layer are strained asymmetrically.[15,17]

To understand the impact of these different strain models on the refinement, we tried both models on our experimental data. We found that the quality of fit (smaller values of χ^2) is significantly better when using the inhomogeneous and asymmetric strain model. Consequently, the discussion below focuses mainly on this model.

Among the (0 0 0), (0 0 2), (0 0 4), and (0 0 6) diffraction series, the (0 0 0) diffraction does not readily provide atomic scale information such as the d spacing and the number of atomic layers. The (0 0 6) XRD series is superior to the remaining two in angular resolution, but has less intensity resulting in a poor signal to noise ratio. Although the (0 0 2) series yields approximately the same intensity as the (0 0 4) series, it does not provide the same high angular resolution as the (0 0 4) series. Weighing all factors, we focus most attention on the (0 0 4) series. Figure 3(a) shows an example of a (0 0 4) refinement and experimental data, demonstrating the high quality refinement that can be achieved. In Fig. 3(b), refinement results from the homogeneous and symmetric model and from the inhomogeneous and asymmetric model are compared. Note that the refinement results from the latter model more closely match the experimental data, reproducing the absence of +third, +fifth, and +seventh order peaks.

B. Experimental and refinement results

The superlattice periodicity can be obtained in a straightforward way from a linear fit based on Bragg's law.[15] In Fig.

TABLE I. The description of all samples studied in this article. All thickness values are given as expected from the growth process (L_{IF}=interfacial layer thickness; 1, 2 refer to the interface between InAs and GaSb, and GaSb and InAs, respectively).

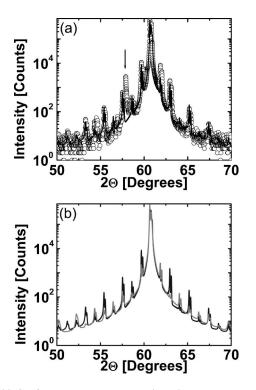| Sample No.	Wafer type	GaSb buffer thickness (Å)	InAs layer thickness (Å)	L_{IF} 1 (Å)	GaSb layer thickness (Å)	L_{IF} 2 (Å)	No. of bilayers
1	GaSb (001)	10 000	0	0	0	0	N/A
2	GaSb (001)	10 000	49	0	40	0	20
3	GaSb (001)	10 000	49	2.85	40	2.85	20
4	GaSb (001)	10 000	49	3.42	40	3.42	20
5	GaSb (001)	10 000	49	3.99	40	3.99	20
6	GaSb (001)	10 000	49	5.13	40	5.13	20

FIG. 3. (a) Θ-2Θ scanning results in the (0 0 4) range of sample 3. The black circles are experimental data and the solid curve is fitted. The fit reproduces the experimental data very well except in the area denoted by an arrow, which is caused by the GaSb buffer layer. (b) Comparison of refinement results for sample 3 using the two strain models: The gray curve is obtained using the homogeneous and symmetric strain model; the black curve is obtained using the inhomogeneous and asymmetric strain model. Note that the latter reproduces the absence of +third, +fifth, and +seventh order peaks.

4(a), the values obtained by this technique (Λ_1, x axis) are plotted against the values obtained using our inhomogeneous and asymmetric strain refinement model (Λ_2, y axis). As the figure shows, Λ_1 and Λ_2 have very high correlation. Based on Bragg's law, the average d spacing of superlattices is given by
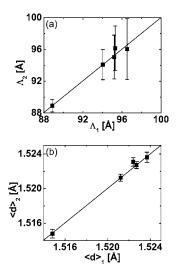

FIG. 4. (a) Correlation of periodicity Λ derived from Bragg's law (Λ_1) and from our inhomogeneous and asymmetric strain refinement model (Λ_2). The error bars are determined by discrete roughness as defined by Fullerton *et al.* (Ref. 15) (b) Correlation of average d spacing of the superlattices between the values from Bragg's law ($\langle d \rangle_1$) and the values from our inhomogeneous and asymmetric strain refinement model ($\langle d \rangle_2$).
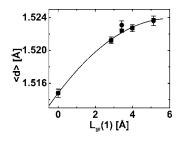

FIG. 5. Average d spacing of the superlattice ($\langle d \rangle$) vs nominal interfacial layer thickness [$L_{IF}(1)$]. The squares represent values from Bragg's law; the circles represent values from the inhomogeneous and asymmetric strain refinement model.

$$\langle d \rangle = \frac{N_{InAs}d_{InAs} + N_{GaSb}d_{GaSb}}{N_{InAs} + N_{GaSb}}.$$

Figure 4(b) shows that there is also a high correlation between the d-spacing values from Bragg's law ($\langle d \rangle_1$) and the values from our inhomogeneous and asymmetric strain refinement model ($\langle d \rangle_2$). Figure 5 displays the change in the average d spacings of the superlattices as a function of the InSb-like interfacial layer thickness.

Figures 4(a), 4(b), and 5 prove that SUPREX refinement based on the asymmetric inhomogeneous model is in good quantitative agreement with values calculated earlier by standard methods.[5,11,15]

However, the complete characterization of a superlattice structure requires determination of additional parameters which may also affect the physical properties. Besides the overall periodicity and average d spacing, detailed information of each constituent layer is essential to understand the superlattice band structure, which determines physical properties such as the photoresponse and transport. These additional parameters cannot be obtained simply from the experimental data and this issue has not been satisfactorily discussed in previous studies.[8,11] The SUPREX refinement reproduces real x-ray diffraction data including contributions from samples and apparatus. The refinement procedure automatically adjusts fitting parameters to lead to a minimized deviation of the refined curve from the XRD profile. The full experimental curve provides a strict limitation on the refined parameters. This constraint assures that detailed structural parameters of the individual constituent layers are obtained, thus providing a complete structural picture. Most other approaches do not use information from the full data set.[3,11] Instead, they focus on the position and intensity of the diffraction peaks. It is important to realize that structural information resides in the full spectrum including peak shoulders and absence of diffraction peaks, commonly ignored. Thus SUPREX extracts structural parameters using the full spectrum rather than selected intensities.

Figure 6(a) gives the thickness derived from the SUPREX refinement of the InAs and GaSb constituent layers. Comparing to Table I, we find that the values agree well with those anticipated from the growth process. The average d spacing of the constituent InAs and GaSb layers vary with the different InSb-like interfacial layers, as demonstrated in Fig. 6(b). Without the InSb-like interfacial layer, both InAs and GaSb layers are slightly compressively strained in the z direction.
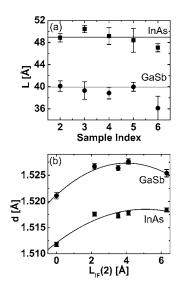
FIG. 6. (a) Thickness of individual SL layers (L) vs sample number. The squares and the circles indicate the thickness of the InAs and GaSb constituent layers from refinement, respectively. (b) Refinement average d spacing of constituent layers (d) vs refinement thickness of interfacial layer [$L_{IF}(2)$]. The squares are values for the InAs layer and circles are values for the GaSb layer.

The InAs lattice exhibits tensile strain in the in-plane direction to match the GaSb buffer lattice, causing compressive strain along the interplanar direction due to the Poisson effect.[18] Figure 7 illustrates the mechanism of this compressive strain. Misfit dislocations will form to relieve in-plane strain if the InAs layer thickness is beyond 2000 Å, which is far thicker than our samples.[19] In our studies, an InSb-like interfacial layer of 2.85 Å nominal thickness, significantly decreases the separation between the zeroth order (or center) peaks (Fig. 2, arrows B and C) of the superlattice and that of the GaSb buffer layer. Thicker InSb-like interfacial layers behave similar to the 2.85 Å thick layer; however, a nominal 5.13 Å thick InSb-like interfacial layer appears to slightly overcompensate the lattice mismatch between the InAs and GaSb layers. An optimal superlattice structure can be achieved by controlling the thickness of the InSb-like interfacial layers. A structure with larger d spacing such as the InSb-like interfacial layers may alleviate the d-spacing "deficit" and relieve the vertical strain. However, thick InSb-like interfacial layers with a considerably larger d spacing than those of the InAs and GaSb layers make superlattice heteroepitaxy unfavorable. A similar qualitative conclusion has been mentioned in a previous study,[11] but no quantitative results related to the thickness of the InSb-like interfacial layers were given.

The SUPREX derived continuous roughness of all superlattice samples is less than 0.06 Å, which can be ignored. The discrete roughness of InAs and GaSb layers varies from 0.7 to 1.4 Å and from 0.6 to 1.7 Å, respectively. Our SU-PREX refinement determined that samples with a thick interfacial layer have a greater amount of discrete roughness than samples with an abrupt interfacial layer. However, a convincing quantitative relation between the discrete roughness and the interfacial layer thickness of all samples is unavailable. The thicknesses of the InSb-like interfacial layers from our SUPREX refinement are given in Fig. 8(a) and these values are
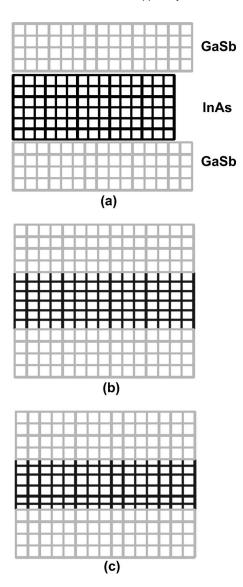

FIG. 7. Schematic diagrams illustrating how interplanar strain occurs in a lattice matched epitaxial SL. (a) The bulk d spacing of InAs is slightly smaller than that of GaSb. In a lattice matched epitaxial SL, the in-plane d spacing of InAs is increased to match that of GaSb, causing a d spacing compression in the out-of-plane direction. This d spacing compression is shown for the homogeneous and symmetric strain model (b) and the inhomogeneous and asymmetric strain model (c).

also close to those expected from the growth process.

The lattice constant and the electron density of the interdiffusion region depend on the parameters of the InAs and GaSb layers. Our approach cannot give detailed chemical composition information of the interfacial layers. The only structural information we can derive about this region is the local d spacing, which is determined by the strain profile across the layer boundary. The local d spacing in the interdiffusion layer can shed some light on its chemical composition. Note that the binary compounds of In, As, Ga, and Sb can be InAs, InSb, GaAs, and GaSb. InAs and GaSb have very similar interplanar d spacing and electron density, while InSb and GaAs have the largest and smallest d spacings, respectively. If the average d spacing in the interdiffusion layer is larger than those of InAs and GaSb, we suggest that the corresponding interfacial layer is InSb like. If the refinement shows a smaller d spacing, the chemical composition is
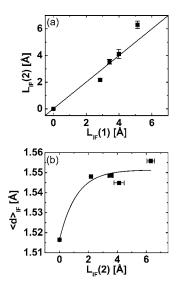
FIG. 8. (a) Correlation between the thickness of the InSb-like interfacial layer from refinement using the inhomogeneous and asymmetric strain model [$L_{IF}(2)$] and the nominal thickness of the InSb-like interfacial layer [$L_{IF}(1)$]. Due to the limitation of our current model, these values can only approximately reflect the actual thickness. (b) The refinement values for the average d spacing of interfacial layers ($\langle d \rangle_{IF}$) vs the thickness of interfacial layers [$L_{IF}(2)$].

possibly GaAs-like. Figure 8(b) shows the refinement average d spacing in the interdiffusion region for the samples listed in Table I. The average d spacing for all samples containing an interfacial layer is larger than those of InAs and GaSb, consistent with the assumption that the interface layers are InSb like. The InAs and GaSb constituent layers have very small x-ray diffraction contrasts because of the similar lattice constant and electron density (scattering factor). The InSb-like interfacial layer, modeled as interdiffusion, is also difficult to differentiate from the remainder of the superlattice. The interdiffusion-related parameters are very sensitively correlated with other structural parameters, which makes it difficult to achieve a stable refinement. We initially fix the interdiffusion parameters in the fitting process and allow the other parameters to achieve stable values. Finally, we release the confinement to interdiffusion and let these parameters vary freely. Following this strategy, we are able to avoid unphysical fits.

C. Absence of odd order peaks

Figure 2 shows that the satellite peaks of order +third, +fifth, and +seventh are absent for samples 3, 4, 5, and 6, while the +first order peak is present. Under special circumstances, lateral compositional modulation[9,10] (LCM) can cause this effect. To investigate this further, we performed Ω-Θ/2Θ 2D x-ray scans which give in-plane structural information. Our data show that at different Φ angles, no diffraction intensity modulation exists along the Ω direction (Fig. 9), which would be expected for samples with LCM. This strongly suggests that the absence of peaks in the samples is unrelated to LCM. We found, however, that we can reproduce the experimental spectra by including inhomogeneous, asymmetrical strain into the refinement model. Summarizing all of our refinement results, we find that a
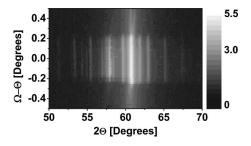

FIG. 9. Two-dimensional Ω-Θ/2Θ scan in the (0 0 4) range for sample 3. The grayscale indicates the XRD intensity on a logarithmic scale.

uniformly strained model results in fits with error as low as about 7%, while the inhomogeneous, asymmetrical strain model reduces the error to about 4%. In addition, the inhomogeneous, asymmetrical strain model simulates well the absence of +third, +fifth, and +seventh order peaks, beyond the ability of the uniformly strained model. This implies that our superlattices are inhomogeneous and asymmetrically strained.

D. Structural coherence length

Herres *et al.*[11] discussed a method to determine the x-ray coherence (grain size) length along the normal and tangential directions of InAs/GaSb superlattices on GaAs substrates. The zeroth order (SL center) peaks for these samples do not overlap with the GaAs (0 0 4) peaks, which allows for measurement of the zeroth order satellite peak full width at half maximum (FWHM) directly from raw x-ray data. However, our InAs/GaSb superlattices are grown on GaSb substrates and the zeroth order peaks are always very close to the GaSb (0 0 4) peaks, complicating the determination of the zeroth order satellite peak FWHM. Although high-resolution x-ray diffraction (HRXRD) may improve the angular resolution significantly, this peak overlap problem is still not entirely solved. We have developed a technique to derive the zeroth order peak FWHM from higher order satellite peaks. The details of this technique are given in Appendix B. Figure 10(a) shows the FWHM of higher order satellite peaks of a given sample, which may be easily obtained from a Θ-2Θ scan. The zeroth order peak FWHM [indicated by arrows in Figs. 10(a) and 10(b)] is obtained from a second order polynomial fit to the data. All zeroth order peak FWHM of the (0 0 2), (0 0 4), and (0 0 6) series can be restored by this method. A similar analysis can be performed on the Ω-Θ data (rocking curve). The solid squares in Fig. 10(b) represent the FWHM of high order peaks from Ω-Θ data and the hollow square represents the FWHM of the GaSb buffer peak. The coherence length in the normal direction is calculated and plotted against the thickness of the InSb-like interfacial layer in Fig. 11. When the superlattice has an InSb-like interfacial layer of about 2.2 Å thick, the superlattice is found to have the longest coherence length (largest grain size in the normal direction). When the thickness of the InSb-like interfacial layers is greater than about 5 Å, the coherence length in the z direction drops significantly. We did not find any relationship between the thickness of the InSb-like interfacial layers and the coherence length in the xy direction.
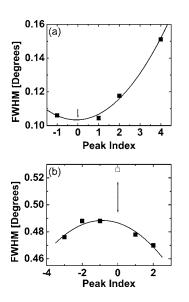
FIG. 10. (a) FWHM of higher order satellite peaks of one superlattice vs their order Θ-2Θ coupled scan). (b) FWHM of higher order satellite peaks of the superlattice vs their order (Ω-Θ coupled scan). The solid lines are polynomial fits to the data, which help determine the FWHM of the zeroth order peaks. The solid squares indicate the FWHM of higher order satellite peaks and the empty square indicates the FWHM of the GaSb buffer layer peak.

IV. CONCLUSION

The average d spacing of InAs/GaSb superlattices increases with insertion of InSb-like interfacial layers between the InAs and GaSb. SUPREX refinement reveals that an InSb-like interfacial layer of nominal thickness $\geq$2.85 Å compensates for the lattice mismatch between InAs and GaSb layers. The average d spacings of individual InAs and GaSb constituent layers are nearly constant as a function of the thickness of the interfacial layer as long as its thickness is greater than 2.85 Å. The SUPREX method provides not only the average d spacing but also the thickness of individual InAs and GaSb layers with high accuracy. The thickness of the interfacial layers can also be estimated and the refined values for the local d spacing across the InAs and GaSb boundary support the assumption that the interfacial layers are InSb like. The thicknesses of individual InAs, GaSb, and interfacial layers derived with SUPREX are well correlated with nominal values expected from the growth process.

In conclusion, we have used the SUPREX structural refinement method to obtain lattice parameters, roughnesses, and strain profiles in InAs/GaSb superlattices.

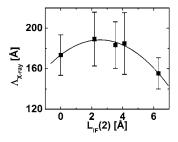The structural coherence length or grain size was ob-

FIG. 11. Structural coherence length ($\Lambda_{x\text{-ray}}$) in the z direction obtained from grain size calculations (Ref. 11) based on the FWHM of the zeroth order peaks vs refinement thickness of interfacial layers [$L_{\text{IF}}(2)$].

tained from the zeroth order superlattice peak FWHM even for samples where this peak is not resolved. Superlattices with mismatch-compensated lattices have longer coherence lengths, but overcompensation greatly reduces the coherence.

2D XRD results exclude the possibility that a lateral compositional modulation causes the absence of odd order satellite peaks in these types of superlattices. SUPREX refinement proves that a model with an inhomogeneous and asymmetric strain profile in the z direction can reasonably describe the details of the full XRD data.

ACKNOWLEDGMENTS

APPENDIX A: DESCRIPTION OF THE SUPREX APPROACH AND APPLIED MODELS

Superlattice refinement by x-ray diffraction, or SUPREX, was developed[12–15] for quantitative structural refinement of superlattices and thin films from x-ray diffraction data. SUPREX is a "refinement" method, as opposed to a simulation, which provides accurate values for lattice parameters and structural disorder. In a refinement, the average atomic structure of the superlattice along with structural disorder are incorporated into a general kinematical diffraction model, which is used in conjunction with a nonlinear fitting algorithm to fit the entire x-ray diffraction profile. Both lattice constants and disorder parameters can be determined from this method. A detailed description of the method[13–15] is beyond the scope of this paper, and the software is available as free download from http://ischuller.ucsd.edu/Suprex.html

Both the homogeneous and symmetric strain model and the inhomogeneous and asymmetric strain model mentioned in this article are based on the standard A/B model included in the SUPREX software package. Since epitaxially grown crystalline InAs/GaSb superlattices with high quality were obtained, a crystalline-crystalline mode of the standard A/B model is selected. The "ideal" superlattice consists of repeated, alternating layers of A and B. In a "real" superlattice, the different layers (A and B) are separated by some kind of an interface. Even if the "bulk" of each A and B layer is perfect, the interface can have imperfections from interdiffusion, discrete disorder, or continuous disorder (roughness). A schematic diagram (Fig. 12) shows how strain is introduced into one of the layers of the standard model. The number of monolayers of layer A is given as N_A. The quantities d_A, Δd_{A1}, and Δd_{A2} are defined as the d spacing in the center layer A, and the strain at the first monolayer nearest to the interface on the lower and upper sides, respectively. α is a constant that characterizes the exponential strain decay from the interface and is typically assumed to be 0.5. Equivalent terms are also defined for layer B. The d spacings at three monolayers closest to the interface are given in Fig. 12. The average d spacing of a constituent layer can be determined

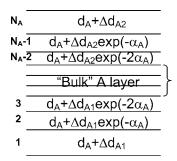| N_A	$d_A + \Delta d_{A2}$
$N_A - 1$	$d_A + \Delta d_{A2} \exp(-\alpha_A)$
$N_A - 2$	$d_A + \Delta d_{A2} \exp(-2\alpha_A)$
	"Bulk" A layer
3	$d_A + \Delta d_{A1} \exp(-2\alpha_A)$
2	$d_A + \Delta d_{A1} \exp(-\alpha_A)$
1	$d_A + \Delta d_{A1}$

FIG. 12. Schematic diagram of the strain for a single constituent layer A of the superlattice used in the refinement. (Please see Appendix A for a definition of the variables.)

by the sum of d spacings inside it ("thickness of one constituent layer") divided by the average number of monolayers as follows:

$$\langle d \rangle = \frac{\left[\sum_{i=0}^{2} \Delta d_1 \exp(-i\alpha_1) + \sum_{i=0}^{2} \Delta d_2 \exp(-i\alpha_2) + Nd \right]}{N}.$$

The discrete roughness of each constituent layer is given as the standard deviation of the number of monolayers multiplied by the d spacing, $\sigma_N d$. Chemical interdiffusion can be introduced into the standard model and a symmetric interdiffusion about the interface is assumed here. Two parameters determine the amount of interdiffusion and the interdiffusion depth. The thickness and average d spacing of the interdiffusion layer were obtained from the refined values of strain profile and interdiffusion parameters.

The *inhomogeneous and asymmetric* strain model assumes bulk d spacing at the center of each layer and a varying strain profile, which can be different at each interface. The *homogeneous and symmetric* strain model assumes that the d spacing may be different from the bulk value, but is constant throughout a layer.

In general, the structural refinement strategy can be divided into five major steps:

(1) Start by assuming a perfect superlattice structure. Using the nominal individual layer thicknesses, bulk lattice constant, and modulation length derived from the intervals between satellite peaks,[15] an initial simulation profile is generated. Interdiffusion parameters are also introduced to reflect the additional contribution by the InSb-like interfacial layers.

(2) A strain profile, representing the distortion near the interface between two layers, is introduced. After this, the shape and intensity of the simulation greatly improved. Roughness is subsequently included to suppress the redundant oscillations, and a Lorentzian doublet is added to the fitting profile to simulate the main GaSb buffer peak. The experimental curve is then initially simulated qualitatively, without attempting to reach the ultimate, smallest χ^2.

(3) In addition to the expected GaSb features, our Te-doped GaSb wafers contained features related to the Cu K_β line, as is indicated by arrow A in the bottom curve of Fig. 2. Satisfactory simulations can be achieved with the above approach except in the areas near these spectral features. To avoid complications from the presence of these features, we removed the portions of the data containing these features by drawing an approximated background in their place. The data are then treated as a GaSb-buffer-free data set.

(4) Further high accuracy fitting is carried out to the experimental data by including a strain profile and thickness of the constituent layers to achieve the lowest possible fitting error χ^2. Once these fitting parameters are stable, the interdiffusion parameters are adjusted to reflect the local chemical intermixing and scattering factor change near the interfaces.

(5) Structural parameters such as the individual average d spacing, the statistical distribution of the thicknesses of the InAs and GaSb layers, and the thickness of the transitional interfacial layer are calculated.

APPENDIX B: CENTRAL SATELLITE PEAK FWHM DETERMINATION IN THE NORMAL DIRECTION

The InAs/GaSb SL samples studied in this paper were grown on a 1 μm thick GaSb (0 0 1) buffer layer, which was epitaxially grown on top of Te-doped GaSb (0 0 1) substrates. The SL zeroth order or central peak is not resolved from the GaSb buffer and GaSb substrate intrinsic peaks, which makes it difficult to determine the FWHM of the zeroth order SL peak directly from XRD data.

According to the diffraction theory of superlattices,[15] the FWHM is determined by the material's Debye-Waller factor, continuous disorder (noncrystalline origin), and discrete disorder (crystalline origin). Only discrete disorder modifies the FWHM according to the order of satellite peaks. Our derivation shows that when the broadening contribution by discrete disorder is excluded from the original experimental data, the zeroth order peak FWHM can be obtained.

According to the theory, the high angle peaks can be indexed about the average lattice constant $\langle d \rangle$ by

$$\frac{2 \sin \Theta_m}{\lambda_{\text{x-ray}}} = \frac{1}{\langle d \rangle} \pm \frac{m}{\Lambda} = \frac{N_A + N_B \pm m}{\Lambda},$$

where $\langle d \rangle = (N_A d_A + N_B d_B)/(N_A + N_B)$, $\Lambda = N_A d_A + N_B d_B$, and m is the index of satellite peaks. The variation in $\langle d \rangle$ is obtained from

$$\delta \left(\frac{2 \sin \Theta_m}{\lambda_{\text{x-ray}}} \right) = \delta \left(\frac{N_A + N_B \pm m}{\Lambda} \right) + \Delta,$$

where Δ is the order-independent broadening caused by factors other than discrete order. Introducing the discrete disorder in N_A and N_B as δN_A and δN_B gives

$$\frac{2 \cos \Theta_m}{\lambda_{\text{x-ray}}} \delta \Theta_m = \frac{(d_B - d_A)(N_B \delta N_A - N_A \delta N_B)}{\Lambda^2}$$

$$\mp m \frac{(d_A \delta N_A + d_B \delta N_B)}{\Lambda^2} + \Delta.$$

Because $\cos \Theta_m$ is nearly a constant over a small range around the major diffraction peak, the intercept of a linear fit

of $\delta\Theta_m$ vs m gives us the value of the first term on the right hand side of the equation, which is also the FWHM of the zeroth order peak. Since the actual experimental data are determined by a very complicated profile, we choose a second order polynomial fit instead of a linear fit to calculate the zeroth order peak FWHM, because the statistical error does not add linearly.

[1] D. L. Smith and C. Mailhiot, J. Appl. Phys. **62**, 2545 (1987).

[2] D. L. Smith and C. Mailhiot, Surf. Sci. **196**, 683 (1988).

[3] H. Mohseni, E. Michel, J. Sandoen, M. Razeghi, W. Mitchel, and G. Brown, Appl. Phys. Lett. **71**, 1403 (1997).

[4] H. Mohseni, A. Tahraoui, J. Wojkowski, M. Razeghi, G. J. Brown, W. C. Mitchel, and Y. S. Park, Appl. Phys. Lett. **77**, 1572 (2000).

[5] H. J. Haugan, F. Szmulowicz, G. J. Brown, and K. Mahalingam, Appl. Phys. Lett. **84**, 5410 (2004).

[6] Y. Wei and M. Razeghi, Phys. Rev. B **69**, 085316 (2004).

[7] F. Szmulowicz, H. Haugan, and G. J. Brown, Phys. Rev. B **69**, 155321 (2004).

[8] H. J. Haugan, L. Grazulis, G. J. Brown, K. Mahalingam, and D. H. Tomich, J. Cryst. Growth **261**, 471 (2004).

[9] D. W. Stokes, R. L. Forrest, J. H. Li, S. C. Moss, B. Z. Nosho, B. R. Benett, L. J. Whitman, and M. Goldenberg, J. Appl. Phys. **93**, 311 (2003).

[10] C. Pearson, C. Dorin, J. Mirecki Millunchick, and B. G. Orr, Phys. Rev. Lett. **92**, 056101 (2004).

[11] N. Herres *et al.*, Phys. Rev. B **53**, 15688 (1996).

[12] M. B. Stearns, Phys. Rev. B **38**, 8109 (1988).

[13] I. K. Schuller, Phys. Rev. Lett. **44**, 1597 (1980).

[14] W. Sevenhans, M. Gijs, Y. Bruynseraede, H. Homma, and I. K. Schuller, Phys. Rev. B **34**, 5955 (1986).

[15] E. E. Fullerton, I. K. Schuller, H. Vanderstraeten, and Y. Bruynseraede, Phys. Rev. B **45**, 9292 (1992).

[16] J. R. Waterman, B. V. Shanabrook, R. J. Wagner, M. J. Yang, J. L. Davis, and J. P. Omaggio, Semicond. Sci. Technol. **8**, S106 (1993).

[17] R. Kaspi, J. Cryst. Growth **201/202**, 864 (1999).

[18] C. K. Pan, D. C. Zheng, T. G. Finstad, and W. K. Chu, Phys. Rev. B **31**, 1270 (1985).

[19] B. R. Bennett, Appl. Phys. Lett. **73**, 3736 (1998).